S1 Calculating the value of g

We followed the methods of Pope *et al.* (2016; their Supplement) to calculate the value for the coefficient for the losses in upward and downward travel through the water column (g; m^{-1}) for the red band of Sentinel-2. The relationship from Smith and Baker (1981; their Eq. (5)) states that:

$$K_d = a + \frac{1}{2}b, \tag{S1}$$

where K_d is the diffuse attenuation coefficient for the clearest natural freshwaters, a is the absorption coefficient for pure water, and b is the backscattering coefficient for molecular (Rayleigh) scattering in freshwater.

We then used the relationship from Sneed and Hamilton (2007; their Eq. (3)), which indicates that:

$$g \approx K_d + aD_u, \tag{S2}$$

where D_u is an upwelling light distribution or the reciprocal of the upwelling average cosine (Mobley, 1994). Since $K_d \approx aD_u$ (Maritorena *et al.*, 1994), g can simply be calculated (using measured values of a and b) with the following:

$$g = 2(K_d), \tag{S3}$$

meaning that Eq. (S1) could then be used to derive the following relationship:

$$g = 2(a + \frac{1}{2}b). \tag{S4}$$

For a, we followed Pope *et al.* (2016) and took the value from Pope and Fry (1997; their Table 3) to replace that from Smith and Baker (1981; their Table 1), and, for b, we took the value from Buiteveld *et al.* (1994; their Table 1) for each wavelength of Sentinel-2's red band. This allowed a preliminary g value to be calculated for Sentinel-2's red band by using Eq. (S4) for each wavelength of the red band (from 646–684 nm in 1 nm increments). To derive a final value, following Pope *et al.* (2016), Sentinel-2's spectral response function (ESA, 2017) was used (akin to the data available for Landsat 8 (Barsi *et al.*, 2014)), and an average weighted value was calculated according to the spectral response for each wavelength of the red band.

This produced a final g value for Sentinel-2's red band of 0.8304, which compares with the lower g value for Landsat 8's red band of 0.7507 (Pope *et al.*, 2016).

Table S1: Details of Sentinel-2 Multispectral Instrument images used in the study. Cloud cover was determined from the image metadata, representing the percentage of cloud-covered pixels both within the ice-sheet area and off the ice-sheet edge. Data cover was determined from the image metadata, representing the percentage of the total area of the region (i.e. the area on the ice sheet plus the ice-marginal area) for which satellite data were collected.

Scene ID	UTM zone	Latitude band	Square	Date	Year	Sequence	Cloud cover (%)	Data cover (%)
S2A_OPER_MSI_L1C_DS_MTI__20160502T202602_S20160502T151916_N02.01	22N	W	EC	02 May	2016	0	38.9	100.0
S2A_OPER_MSI_L1C_DS_SGS__20160505T205541_S20160505T152915_N02.02	22N	W	EC	05 May	2016	0	44.7	100.0
S2A_OPER_MSI_L1C_DS_MTI__20160515T203516_S20160515T152912_N02.02	22N	W	EC	15 May	2016	0	5.4	100.0
S2A_OPER_MSI_L1C_DS_SGS__20160518T210306_S20160518T154153_N02.02	22N	W	EC	18 May	2016	0	31.4	38.3
S2A_OPER_MSI_L1C_DS_MTI__20160522T202416_S20160522T151915_N02.02	22N	W	EC	22 May	2016	0	29.8	100.0
S2A_OPER_MSI_L1C_DS_MTI__20160529T201543_S20160529T150918_N02.02	22N	W	EC	29 May	2016	0	66.1	94.3
S2A_OPER_MSI_L1C_DS_SGS__20160601T173946_S20160601T151916_N02.02	22N	W	EC	01 Jun	2016	0	18.1	99.9
S2A_OPER_MSI_L1C_DS_MTI__20160604T203539_S20160604T152915_N02.02	22N	W	EC	04 Jun	2016	0	60.0	99.9
S2A_OPER_MSI_L1C_DS_SGS__20160608T202646_S20160608T150916_N02.02	22N	W	EC	08 Jun	2016	0	16.2	94.2
S2A_OPER_MSI_L1C_DS_MTI__20160611T202435_S20160611T151937_N02.02	22N	W	EC	11 Jun	2016	0	42.5	100.0
S2A_OPER_MSI_L1C_DS_SGS__20160617T192017_S20160617T153910_N02.04	22N	W	EC	17 Jun	2016	0	25.7	38.9
S2A_OPER_MSI_L1C_DS_SGS__20160618T202441_S20160618T151305_N02.04	22N	W	EC	18 Jun	2016	0	46.7	93.2
S2A_OPER_MSI_L1C_DS_MTI__20160621T220258_S20160621T151912_N02.04	22N	W	EC	21 Jun	2016	0	4.3	100.0
S2A_OPER_MSI_L1C_DS_MTI__20160624T203434_S20160624T152911_N02.04	22N	W	EC	24 Jun	2016	0	16.0	100.0
S2A_OPER_MSI_L1C_DS_SGS__20160628T202858_S20160628T150914_N02.04	22N	W	EC	28 Jun	2016	0	0.1	94.0
S2A_OPER_MSI_L1C_DS_MTI__20160701T202434_S20160701T151913_N02.04	22N	W	EC	01 Jul	2016	0	73.3	100.0
S2A_OPER_MSI_L1C_DS_SGS__20160707T192822_S20160707T153908_N02.04	22N	W	EC	07 Jul	2016	0	0.0	38.6
S2A_OPER_MSI_L1C_DS_SGS__20160708T202909_S20160708T151305_N02.04	22N	W	EC	08 Jul	2016	1	1.6	94.2
S2A_OPER_MSI_L1C_DS_SGS__20160711T203749_S20160711T151912_N02.04	22N	W	EC	11 Jul	2016	0	0.1	100.0
S2A_OPER_MSI_L1C_DS_MTI__20160714T203553_S20160714T152910_N02.04	22N	W	EC	14 Jul	2016	0	0.3	99.9
S2A_OPER_MSI_L1C_DS_SGS__20160718T202939_S20160718T150915_N02.04	22N	W	EC	18 Jul	2016	0	23.7	94.2

Scene ID	UTM zone	Latitude band	Square	Date	Year	Sequence	Cloud cover (%)	Data cover (%)
S2A_OPER_MSI_L1C_DS_MTI__20160721T202530_S20160721T151913_N02.04	22N	W	EC	21 Jul	2016	0	0.0	100.0
S2A_OPER_MSI_L1C_DS_SGS__20160724T205100_S20160724T153051_N02.04	22N	W	EC	24 Jul	2016	0	0.0	99.9
S2A_OPER_MSI_L1C_DS_SGS__20160727T192945_S20160727T153910_N02.04	22N	W	EC	27 Jul	2016	0	0.0	38.2
S2A_OPER_MSI_L1C_DS_SGS__20160728T202436_S20160728T151306_N02.04	22N	W	EC	28 Jul	2016	0	63.6	94.3
S2A_OPER_MSI_L1C_DS_SGS__20160731T203724_S20160731T151913_N02.04	22N	W	EC	31 Jul	2016	0	0.0	100.0
S2A_OPER_MSI_L1C_DS_MTI__20160803T203554_S20160803T152910_N02.04	22N	W	EC	03 Aug	2016	0	3.1	100.0
S2A_OPER_MSI_L1C_DS_MTI__20160806T204409_S20160806T153909_N02.04	22N	W	EC	06 Aug	2016	0	14.1	38.1
S2A_OPER_MSI_L1C_DS_SGS__20160807T202758_S20160807T150914_N02.04	22N	W	EC	07 Aug	2016	0	55.9	94.4
S2A_OPER_MSI_L1C_DS_MTI__20160810T202535_S20160810T151912_N02.04	22N	W	EC	10 Aug	2016	0	13.0	100.0
S2A_OPER_MSI_L1C_DS_SGS__20160813T204833_S20160813T153046_N02.04	22N	W	EC	13 Aug	2016	0	0.0	100.0
S2A_OPER_MSI_L1C_DS_SGS__20160817T202447_S20160817T151257_N02.04	22N	W	EC	17 Aug	2016	0	0.7	94.4
S2A_OPER_MSI_L1C_DS_MTI__20160830T202522_S20160830T151909_N02.04	22N	W	EC	30 Aug	2016	0	2.2	100.0
S2A_OPER_MSI_L1C_DS_SGS__20160902T204312_S20160902T153051_N02.04	22N	W	EC	02 Sep	2016	0	0.7	100.0
S2A_OPER_MSI_L1C_DS_SGS__20160906T202733_S20160906T151257_N02.04	22N	W	EC	06 Sep	2016	0	35.9	94.5
S2A_OPER_MSI_L1C_DS_SGS__20160909T203815_S20160909T151907_N02.04	22N	W	EC	09 Sep	2016	0	21.0	100.0
S2A_OPER_MSI_L1C_DS_MTI__20160912T203709_S20160912T152817_N02.04	22N	W	EC	12 Sep	2016	0	0.0	100.0
S2A_OPER_MSI_L1C_DS_SGS__20160915T210159_S20160915T154130_N02.04	22N	W	EC	15 Sep	2016	0	1.7	38.2
S2A_OPER_MSI_L1C_DS_MTI__20160926T201345_S20160926T150955_N02.04	22N	W	EC	26 Sep	2016	0	0.3	93.9

Table S2: Details of Landsat 8 Operational Land Imager images used in the study. Cloud cover was calculated as the percentage of pixels both on and off the ice sheet that were obscured by clouds (i.e. those with a band-6 value > 0.100; Sect. 2.2.1). Data cover was calculated as a percentage of the total area of the region (i.e. the area on the ice sheet plus the ice-marginal area) for which satellite data had been collected. * denotes that the image was used for comparing lake areas calculated from the two satellites and for validating the lake depths from Sentinel-2, but that the image was not used for lake tracking because a contemporaneous higher-resolution, and therefore more favourable, Sentinel-2 image was available.

Scene ID	Path	Row	Date	Year	Cloud cover (%)	Data cover (%)
LC80100112016149LGN01	010	011	28 May	2016	85.9	95.1
LC80080112016151LGN01	008	011	30 May	2016	8.4	72.8
LC80822332016157LGN01	082	233	05 Jun	2016	17.3	100.0
LC80090112016158LGN01	009	011	06 Jun	2016	21.6	100.0
LC80100112016165LGN01	010	011	13 Jun	2016	43.9	95.3
LC80090112016174LGN01	009	011	22 Jun	2016	33.9	100.0
LC80100112016181LGN01	010	011	29 Jun	2016	35.0	95.2
LC80080112016183LGN01	008	011	01 Jul*	2016	60.8	72.6
LC80100112016197LGN01	010	011	15 Jul	2016	21.0	95.1
LC80812332016198LGN01	081	233	16 Jul	2016	19.0	93.7
LC80080112016199LGN01	008	011	17 Jul	2016	5.9	72.8
LC80100112016213LGN01	010	011	31 Jul*	2016	18.5	95.2
LC80080112016215LGN01	008	011	02 Aug	2016	12.2	72.6
LC80090112016222LGN01	009	011	09 Aug	2016	18.4	100.0
LC80100112016229LGN01	010	011	16 Aug	2016	18.3	95.2
LC80080112016231LGN01	008	011	18 Aug	2016	6.5	72.7
LC80080112016247LGN01	008	011	03 Sep	2016	8.8	73.2

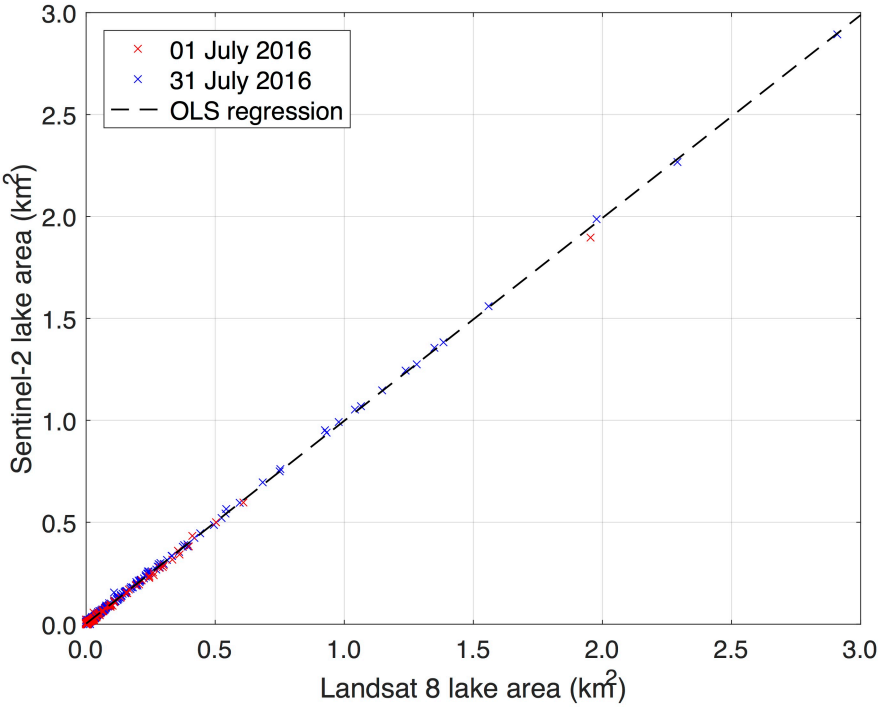

Figure S1: The very strong relationship between Landsat 8 and Sentinel-2 lake areas for the days of overlapping imagery (1 July and 31 July) in 2016. The 594 lake areas used for comparisons were derived using the Normalised Difference Water Index (NDWI) approach with threshold values of 0.25 for both types of imagery. The black dashed line shows an ordinary least-squares (OLS) linear regression, which can explain 99.9% (R^2 = 0.999; p = 0.000) of the variance in the data. The root-mean square error of 0.007 km^2 (i.e. seven Sentinel-2 pixels) between the two sets of lake areas is remarkably small.

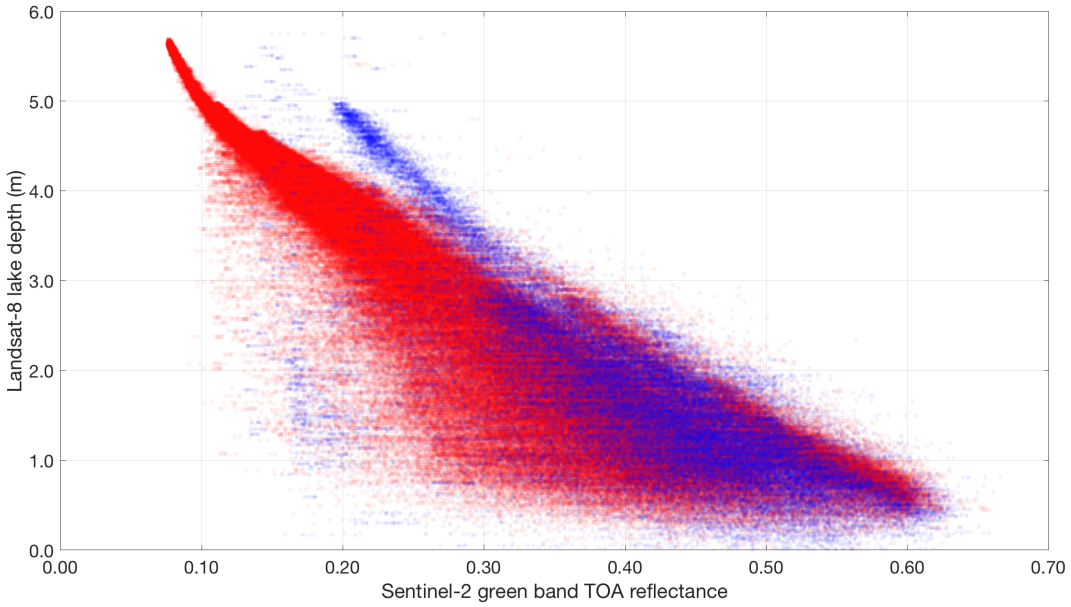

Figure S2: Scatter plot to show the relationship between Sentinel-2 green band top-of-atmosphere (TOA) reflectance and Landsat 8 lake depth for 430,650 data points (blue circles = 1 July; red squares = 31 July).

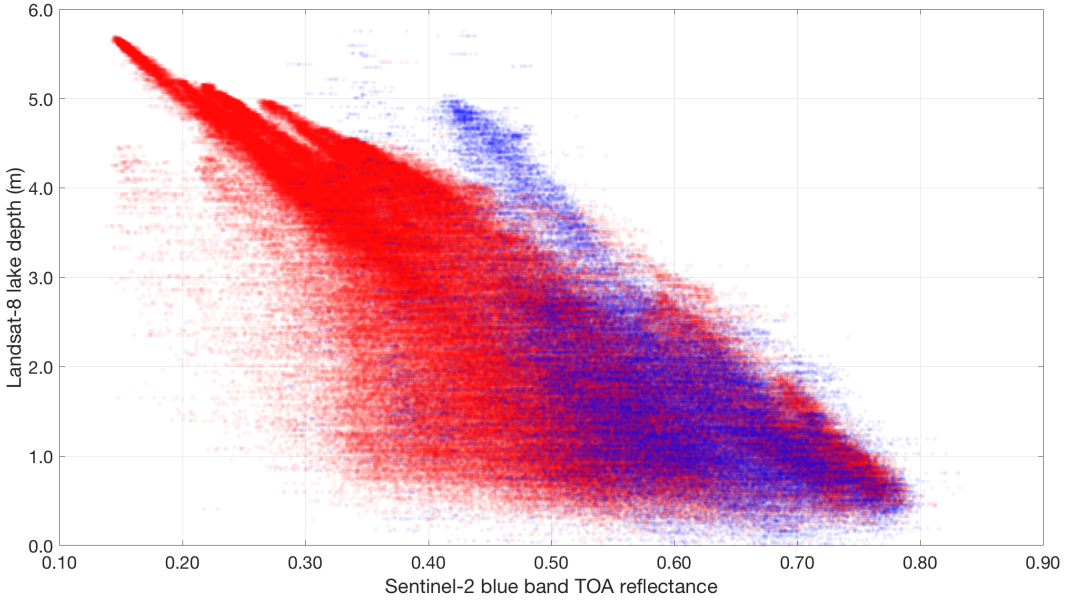

Figure S3: Scatter plot to show the relationship between Sentinel-2 blue band TOA reflectance and Landsat 8 lake depth for 430,650 data points (blue circles = 1 July; red squares = 31 July).

References

Barsi, J. A., Lee, K., Kvaran, G., Markham, B. L., and Pedelty, J. A.: The spectral response of the Landsat-8 Operational Land Imager, Remote Sens., 6, 10232–10251, https://doi.org/10.3390/rs61010232, 2014.

ESA: Sentinel-2 spectral response functions (S2-SRF), accessed 19 February 2018, https://earth.esa.int/web/sentinel/user-guides/sentinel-2-msi/document-library/-/asset_publisher/Wk0TKajiISaR/content/sentinel-2a-spectral-responses, 2017.

Maritorena, S., Morel, A., and Gentili, B.: Diffuse reflectance of oceanic shallow waters: Influence of water depth and bottom albedo, Limnol. Oceanogr., 39, 1689–1703, https://doi.org/10.4319/lo.1994.39.7.1689, 1994.

Mobley, C. D.: Light and water: Radiative transfer in natural waters, Academic Press, San Diego, 1994.

Pope, A., Scambos, T. A., Moussavi, M., Tedesco, M., Willis, M., Shean, D., and Grigsby, S.: Estimating supraglacial lake depth in West Greenland using Landsat 8 and comparison with other multispectral sensors, The Cryosphere, 10, 15–27, https://doi.org/10.5194/tc-10-15-2016, 2016.

Pope, R. M. and Fry, E. S.: Absorption spectrum (380–700 nm) of pure water. II. Integrating cavity measurements, Appl. Opt., 36, 8710–8723, https://doi.org/10.1364/AO.36.008710, 1997.

Smith, R. C. and Baker, K. S.: Optical properties of the clearest natural waters (200–800 nm), Appl. Opt., 20, 177–184, https://doi.org/10.1364/AO.20.000177, 1981.

Sneed, W. A. and Hamilton, G. S.: Evolution of melt pond volume on the surface of the Greenland Ice Sheet, Geophys. Res. Lett., 34, L03501, https://doi.org/10.1029/2006GL028697, 2007.